Journal of Ultrafine Grained and Nanostructured Materials
https://jufgnsm.ut.ac.ir
Vol. 59, No.1, June 2026, pp. 41-48
Print ISSN: 2423-6845 Online ISSN: 2423-6837
DOI: 10.22059/jufgnsm.2026.01.04

Comparative Study of Strontium- and Chromium-Modified PEO Coatings on Mg Alloys for Photocatalytic Degradation of Methylene Blue

Abdelhameed Fardosi[1], Arash Fattah-alhosseini[1,*], Minoo Karbasi[1], Razieh Chaharmahali[1], Burak Dikici[2,*], Mosab Kaseem[3,*]

[1]Department of Materials Engineering, Faculty of Engineering, Bu-Ali Sina University, Hamedan, Iran
[2]Department of Mechanical Engineering, Ataturk University, Erzurum 25240, Turkey
[3]Sejong University, Department of Nanotechnology and Advanced Materials Engineering, Seoul 05006, Republic of Korea

Recieved: 26 November 2025; Accepted: 14 February 2026

[*]Corresponding author, E-mail: a.fattah@basu.ac.ir, burakdikici@atauni.edu.tr, mosabkaseem@sejong.ac.kr

ABSTRACT

In this study, plasma electrolytic oxidation (PEO) coatings were developed on AZ31B Mg alloy under a constant current density of 12 A·dm^{-2} in a phosphate-based electrolyte, with modifications introduced by strontium (Sr) and chromium (Cr) ions. Three coating types were obtained: unmodified (12A), Sr-modified (12A-Sr), and Cr-modified (12A-Cr). All coatings exhibited porous and micro-cracked morphologies, characteristic of oxide ejection and rapid solidification during the PEO process. Grazing-angle X-ray diffraction (GXRD) confirmed the presence of MgO and $ZnAl_2O_4$ phases. Surface characterization revealed that the 12A-Sr coating displayed pronounced hydrophobicity (contact angle ≈115°), attributed to chemical and microstructural modifications that enhanced air entrapment. Photocatalytic experiments demonstrated that all coatings were active under visible light, with the Cr-modified coating showing the highest MB degradation efficiency, followed by the unmodified and Sr-modified samples. Electrochemical impedance spectroscopy (EIS) further indicated that visible light irradiation significantly improved charge transfer, as evidenced by reduced Nyquist arc radii, highlighting efficient electron–hole separation and accelerated interfacial reactions. The results demonstrate that Sr- and Cr-modified PEO coatings hold promise for improving photocatalytic wastewater treatment.

Keywords: *Methylene blue; Photocatalytic; Plasma electrolytic oxidation (PEO); AZ31B Mg alloy.*

1. Introduction

Dyes employed in textile and various other industries represent one of the major contributors to organic pollution, increasingly endangering the environment. During the dyeing process, approximately 1–20% of the dyes manufactured worldwide are lost and released, positioning them as a significant source of organic contamination in textile wastewater [1]. Methylene blue (MB), a cationic dye commonly applied in fabric production, is resistant to environmental degradation and has been linked to cancer, toxicity, and genetic mutations [2,3]. MB dyeing can also lead to fatal serotonin poisoning in humans when ingested in doses exceeding 5 mg/kg, as it inhibits the enzyme monoamine oxidase responsible for serotonin breakdown. It further harms animals living in ecosystems where it is discharged [4]. Major adverse effects of MB can involve serotonin syndrome, disorientation, nausea, elevated blood

pressure, breathing difficulties, damage to red blood cells, headaches, and hypersensitivity reactions [5]. Therefore, water polluted with this dye demands immediate treatment, both to safeguard environmental and human health and to facilitate the reuse of alternative water resources.

Organic-polluted wastewater can be treated using advanced oxidation processes (AOPs), which are promising techniques extensively studied for the degradation of pesticides, antibiotics, organic dyes, and other emerging pollutants. These processes rely on highly oxidizing reactive species such as free radicals ($SO_4\bullet^-$, $OH\bullet$, $O_2\bullet^-$, $Cl\bullet$), strong oxidizing molecules (O_3, $^1O_2$, etc.), and electrons/holes, which degrade organic contaminants via intricate electron transfer pathways [6]. Among AOPs, semiconductor photocatalysis has attracted significant attention in recent years because of its affordability, operational simplicity, and eco-friendly nature [7].

PEO is a recognized industrial method for surface modification, converting metals like aluminum, magnesium, titanium, and their alloys into protective oxide layers. By adjusting the electrolyte composition or incorporating nanoparticles, these coatings can be enriched with additional functional components [8].

Several studies have explored the formation of PEO coatings on Mg alloys to achieve photocatalytic activity and pollutant degradation. For example, Lu et al. investigated the effect of TiO_2 particle concentration and process voltage in a phosphate-based electrolyte on MB degradation under UV light, showing that lower voltage increased TiO_2 incorporation and improved photocatalytic efficiency. Stojadinovic et al. [9] examined Eu_2O_3 nanoparticle concentration in an aluminite-based electrolyte for methyl orange degradation under simulated sunlight, finding that moderate doping enhanced photocatalytic behavior, while excessive doping promoted electron–hole recombination. Similarly, Li et al. [10] studied TiO_2 nanoparticle addition to a phosphate-based electrolyte for MB degradation under visible light, reporting improved photocatalytic activity at lower concentrations but reduced corrosion resistance at higher concentrations due to crack formation.

Although particle and nanoparticle incorporation into the PEO electrolyte is effective for enhancing properties such as corrosion resistance, this approach has limitations. Therefore, the present study aims to improve photocatalytic activity by introducing chromium (Cr) and strontium (Sr) ions into the electrolyte during the formation of PEO coatings. The comparative effects of Sr and Cr modifications, as well as their concentrations, will be systematically investigated to identify optimal conditions for photocatalytic performance.

2. Materials and Methods

2.1. Materials

In this work, AZ31B Mg alloy specimens measuring $20 \times 15 \times 3$ mm^3 served as substrates. The chemicals supplied by Merck included potassium hydroxide (KOH), sodium orthophosphate ($Na_3PO_4{\cdot}12H_2O$), strontium nitrate ($Sr(NO_3)_2$), and chromium nitrate ($Cr(NO_3)_3{\cdot}9H_2O$).

2.2. Fabrication of PEO coatings

A pulsed DC power supply (PM700/7 PRC (IPS)) capable of delivering up to 700 V was employed to perform the PEO process in a two-electrode cell. Before undergoing PEO, the AZ31B alloy samples were polished using sandpaper up to a 1500-grit finish. The sanding process began with 80-grit sandpaper to eliminate cutting marks. The sample was then sequentially polished using a progression of grits: 120, 220, 400, 600, 800, 1000, 1200, and 1500. Crucially, the sample's orientation was rotated vertically when transitioning to each finer grit.

After ultrasonic cleaning in acetone to remove oils, the samples were washed with distilled water and then dried in air. The PEO treatment was carried out with a pulsed DC power source in a two-electrode configuration at a peak voltage of 700 V. In this arrangement, the polished AZ31B specimens functioned as the anode, and a stainless steel cooling unit served as the cathode. The cooling system maintained the electrolyte temperature below 25 °C.

Each specimen underwent PEO for 7 min at a 1 kHz pulse frequency with a 50% duty cycle to obtain uniform coatings. After treatment, the samples were rinsed with distilled water. Table 1 summarizes PEO parameters, including electrolyte composition, current density, and sample codes. The stability of the electrolyte is chiefly determined by the concentration of hydroxide ions (OH^-) present in the solution [1]. As evidenced by the pH measurements of the electrolyte solutions detailed in Table 1, no significant change is observed between the initial state and the state following the Plasma Electrolytic Oxidation (PEO) coating procedure for electrolytes incorporating either $Cr(NO_3)_3$ or $Sr(NO_3)_2$. This observed stability in pH values verifies that the overall conditions of the electrolyte remain constant throughout the process. Therefore, it can be concluded that Sr^{2+} and Cr^{3+} ions do not substantially consume or deplete the available OH^- ions. This is attributed to their tendency to form stable coordination complexes within the phosphate-KOH based system, a finding that is corroborated by the invariant pH measurements recorded before and after the PEO process.

2.3. Characterization of PEO coatings

In this work, the microstructural and surface characteristics of PEO coatings were analyzed with a QUANTA 200 FEI SEM running at 15 kV. Crystalline phases were identified by grazing-incidence X-ray diffraction (GXRD) using an Asenware AW-XDM300 diffractometer with Cu-Kα radiation at 40 kV and 30 mA. Diffraction patterns were processed with PANalytical X'Pert HighScore software, and phase identification was performed using the ICDD database.

2.4. Photodegradation

The photodegradation rate of the MB solution was measured with a UV–Vis spectrophotometer to evaluate the photocatalytic performance of the coating. For this test, a PEO-coated specimen was placed in 30 mL of MB solution at a concentration of 10 mg/L. Illumination was provided by a 100 W LED source (380–780 nm), positioned 10 cm above the solution. Prior to irradiation, the coated sample in MB solution was kept in the dark for 30 min to establish adsorption–desorption equilibrium. Based on the calibration curve, MB photocatalytic performance was evaluated using Eq. 1:

$$PA(\%) = \frac{C_0 - C}{C_0} \times 100 \quad (1)$$

Here, represents the starting concentration of the MB solution, while indicates its concentration after irradiation.

2.5. Wettability Test

Prior to contact angle measurement, sample coatings and substrates were degreased in ethanol using an ultrasonic bath for 5 min, followed by hot air drying. Wettability was examined by placing a 1 µL droplet of distilled water on the sample surface, photographed after 5 s. Contact angles were determined with image analysis software. For each sample, measurements were taken at multiple surface points, and average values are presented.

2.6. Electrochemical impedance spectroscopy (EIS)

EIS serves as an effective technique for analyzing charge transfer behavior under visible light and dark conditions. During photocatalytic degradation, charge transfer and separation are crucial [11,12], and a smaller arc radius in the Nyquist plot indicates reduced charge transfer resistance [13].

Electrochemical measurements were carried out using a three-electrode electrochemical setup, in which a platinum electrode and an Ag/AgCl electrode served as the counter and reference electrodes, respectively. The fabricated coating acted as the working electrode, and all experiments were conducted using a µAutolab Type III/FRA2 electrochemical workstation. EIS measurements were performed at a fixed frequency of 1000 Hz. The electrochemical tests were carried out in an aqueous electrolyte containing 0.5 M Na_2SO_4.

3. Results and Discussions

Figure 1 illustrates the surface morphology of PEO coatings obtained by the PEO technique. The coatings display the typical structure of PEO layers, with open pores encircled by solidified material expelled during processing. The pores are formed from molten discharge matter ejected into the electrolyte, where it quickly solidifies [14,15]. When the current density increases, the coatings display more cracks within the surface layer. Such fine cracking is linked to thermal stresses caused by the rapid solidification of molten oxides during PEO. The incorporation of chromium and strontium did not alter the surface characteristics of the coatings.

GXRD patterns at the capture angle for the coatings are presented in Figure 2 [16]. The presence of Mg (ICDD file number 00-035-0821) peaks indicates partial penetration of GXRD through the porous PEO layer, revealing the underlying substrate due to the limited thickness of the coating.

Table 1- Parameters for PEO: electrolyte composition, current density, and specimen identifiers

Sample identifiers	Current density ($A \cdot dm^{-2}$)	Electrolyte composition	Additive	pH of the Electrolyte
12A	12	5 $g \cdot L^{-1}$ Na_3PO_4 + 3 $g \cdot L^{-1}$ KOH	-	12.65
12A-Sr			0.5 $g \cdot L^{-1}$ $Sr(NO_3)_2$	12.65
12A-Cr			0.5 $g \cdot L^{-1}$ $Cr(NO_3)_3$	12.61

MgO (ICDD file number 00-045-0946) is generated through oxidation of the substrate metal during PEO, while zinc aluminate (ICDD file number 01-073-1961) forms from oxidation of zinc and aluminum in the substrate.

Considering the limited coating thickness and the penetration depth of X-rays, these reflections are attributed to the combined contribution of the PEO-derived oxide layer and the oxidized near-surface region of the AZ31B substrate, where aluminum- and zinc-containing oxides may locally react under the high transient temperatures generated by plasma discharges.

Figure 2 displays diffraction peaks (200) for samples 12A and 12A-Sr, analyzed using a Gaussian fit. The peak for 12A at 42.99° shifts to 42.87° in the Sr-containing coating. This shift arises from the larger ionic radius of Sr^{2+} (0.118 nm) [17] compared to Mg^{2+} (0.072 nm) [17], which increases the spacing between tetragonal crystalline planes, causing the peak to move toward lower angles in accordance with Bragg's Law [18] The observed peak shift cannot be considered direct evidence of Sr^{2+} substitution into the MgO crystal lattice based solely on GXRD data. Additional factors, such as residual stress and defect formation, may also contribute to the observed peak displacement.

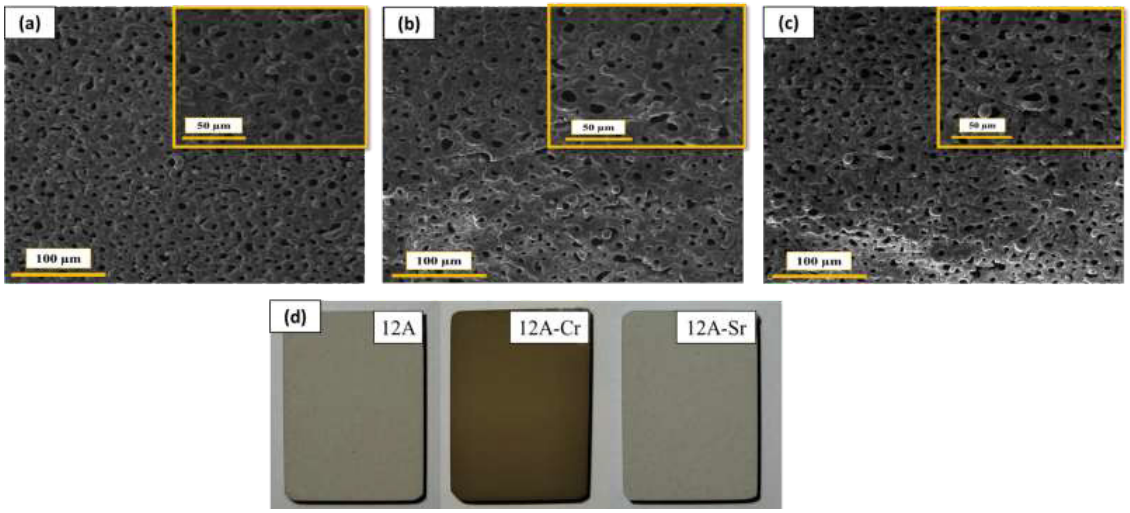

Fig. 1- SEM micrographs of PEO coatings obtained at 12 A·dm^{-2}: (a) 12A, (b) 12A-Cr, (c) 12A-Sr, and (d) digital photos of the fabricated samples [16].

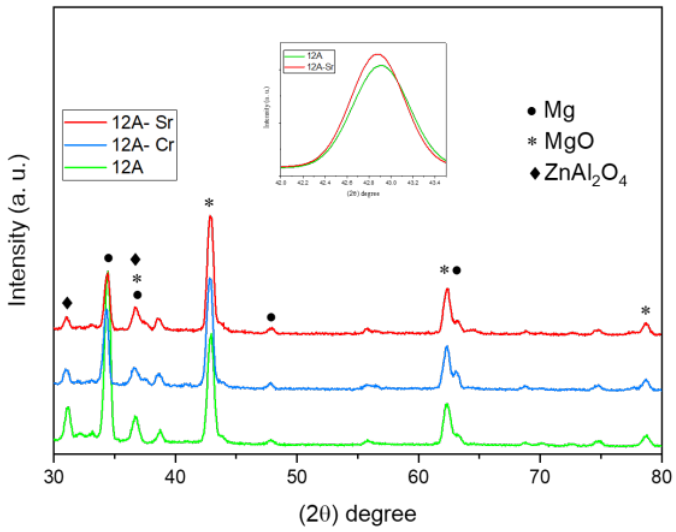

Fig. 2- GXRD spectra of PEO coatings at 12 A·dm^{-2}, with and without Sr and Cr additions [16].

Figure 3 presents the wettability of different PEO coatings. The 12A-Sr specimen shows a contact angle of 115°, demonstrating hydrophobic characteristics [16]. Quantification is generally carried out using contact angle analysis, where a droplet is placed on the surface and the angle formed at the solid–liquid interface is determined [19]. Wettability is an important surface property with broad relevance, especially in biological applications, and influences photocatalytic activity and frictional behavior.

This behavior can be attributed to the combined effects of surface chemistry and microstructural features induced by the PEO process. Incorporation of Sr-containing species, together with the porous and rough morphology typical of PEO coatings, can reduce surface free energy and promote air entrapment within surface asperities, thereby enhancing hydrophobicity.

For oxide coatings, the contact angle is a key thermodynamic parameter that reflects surface wettability during liquid interaction. It is determined by the sessile drop method, where the measured angle defines surface behavior: values above 90° indicate hydrophobicity, while those below 90° correspond to hydrophilicity. Hydrophilic surfaces encourage droplet spreading, resulting in enhanced wettability, while hydrophobic surfaces lead to droplet beading. In contrast, superhydrophobic surfaces characterized by contact angles greater than 150° show almost complete liquid repellency with minimal adhesion [20,21].

Figure 4 shows the surface roughness results [16]. Analysis confirms that all coatings possess Ra values above 1 μm [22,23]. This roughness originates from micro-discharge-driven growth, in which intense plasma discharges encourage thicker oxide formation and generate circular pores that define the surface morphology. The development of roughness in PEO coatings is influenced by multiple interconnected factors. When high voltage is applied in the electrolyte, micro-discharges form at localized points on the substrate, generating plasma channels with temperatures exceeding the vaporization threshold of the metal. This results in the violent expulsion of molten and vaporized material. Importantly, the addition of $Sr(NO_3)_2$ to the electrolyte leads to a reduction in overall surface roughness.

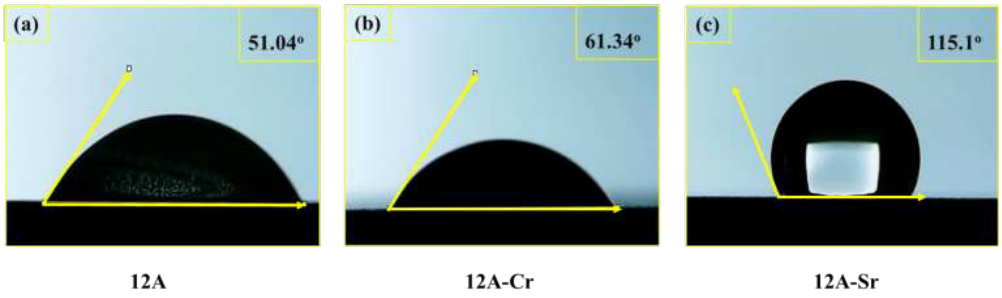

Fig.3- Contact angle results of PEO coatings at 12 A·dm^{-2}, with and without Sr and Cr additions [16].

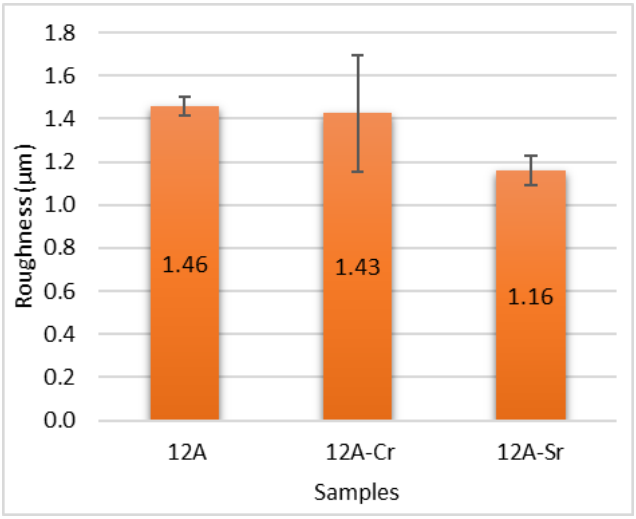

Fig.4- Surface roughness (Ra) of PEO coatings at 12 A·dm^{-2}, with and without Sr and Cr additions [16].

Sample 12A exhibits a moderate contact angle, reflecting a relatively weak interaction between the surface and water, with a moderate roughness factor. In the case of 12A-Cr, the higher contact angle indicates enhanced water repellency, likely due to chemical modification of the surface by Cr, as roughness remained nearly unchanged. The 12A-Sr sample demonstrates a significantly larger contact angle, signifying strong hydrophobicity. Although its surface roughness is slightly reduced, the Cassie–Baxter model appears more suitable here, since Sr alters the surface structure to improve air entrapment [24,25]. The combined influence of surface chemistry and minor roughness variation contributes to the pronounced hydrophobic behavior.

Figure 5 demonstrates that the PEO coating possesses photocatalytic activity, as shown by the progressive degradation of MB dye. The results confirm that no degradation occurred in the dark, and only limited dye breakdown was observed under light exposure alone, highlighting that the primary mechanism is photocatalysis by the bio-coating on the Mg surface.

Incorporating Sr and Cr into the electrolyte did not significantly boost photocatalytic efficiency, although Cr showed a more beneficial effect than Sr. The apparent kinetic constants (k_{app}) for 12A-Cr and 12A are higher than those for 12A-Sr, confirming stronger activity. Among the tested coatings, 12A-Cr demonstrates the highest photocatalytic performance.

In contrast, 12A-Sr displayed weaker photocatalytic behavior compared to the other samples. This reduced activity is likely linked to its large contact angle, which limits contact between the MB dye solution and the coating surface, thereby diminishing photocatalytic effectiveness.

In general, a reduced arc radius in the Nyquist plot is associated with more efficient electron–hole separation and faster charge transfer at the surface. To clarify this behavior, Nyquist plots were obtained for each sample under both visible light and dark conditions. The results reveal that the arc radius under visible light is markedly smaller than in darkness, demonstrating that illumination enhances electron transfer efficiency (Figure 6).

4. Conclusion

In this study, PEO coatings were successfully fabricated on AZ31B Mg alloy under constant current conditions, with modifications introduced by strontium (Sr) and chromium (Cr) ions. All coatings, whether unmodified (12A), Sr-modified (12A-Sr), or Cr-modified (12A-Cr), exhibited the typical porous and micro-cracked morphologies that result from molten oxide ejection and rapid solidification during the PEO process. Grazing-angle X-ray diffraction (GXRD) analysis confirmed the formation of magnesium oxide and zinc aluminate phases within the coatings. Surface characterization revealed that the Sr-modified coating displayed pronounced hydrophobicity, with a contact angle of approximately 115°, which can be attributed to chemical and microstructural modifications enhancing air entrapment in a Cassie-Baxter state.

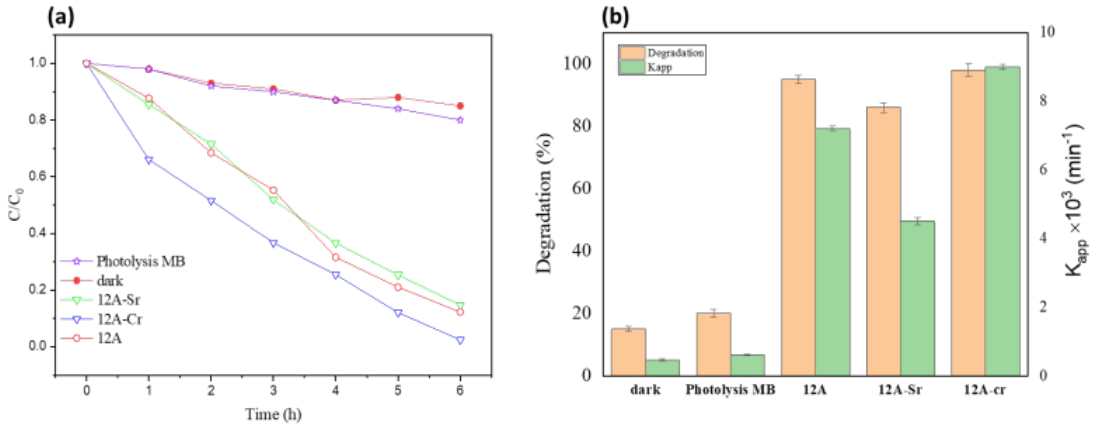

Fig.5- (a) MB decolorization of PEO coatings in dark and under visible light, (b) kinetic constants for MB photocatalytic decolorization.

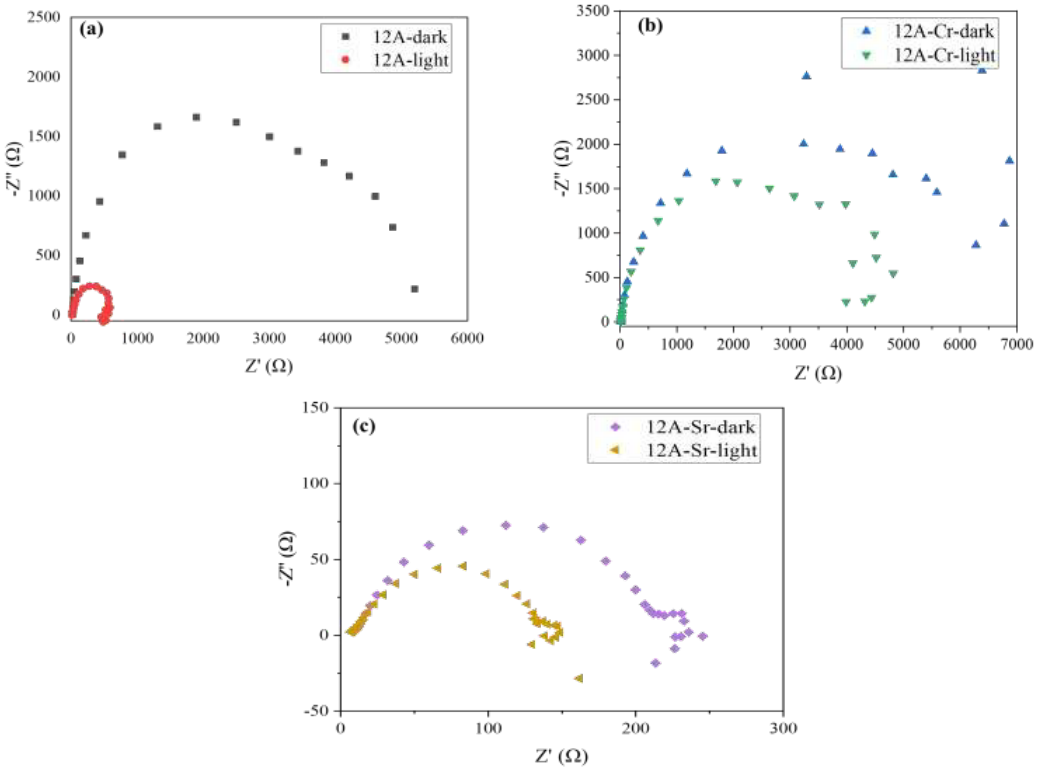

Fig.6- EIS plots of PEO coatings at 12 A·dm^{-2}, with and without Sr and Cr, under light and dark.

Photocatalytic experiments demonstrated that all coatings were active in the degradation of methylene blue under visible light irradiation. Among the samples, the Cr-modified coating exhibited the highest photocatalytic efficiency, followed by the unmodified coating and then the Sr-modified coating. This trend is likely influenced by the larger contact angle of the Sr-modified surface compared to the other samples. Electrochemical impedance spectroscopy (EIS) performed under both light and dark conditions further confirmed that visible light irradiation significantly enhances charge transfer efficiency. The reduced arc radius observed in Nyquist plots under illumination indicates more effective electron–hole pair separation and accelerated interfacial charge transfer, which are essential for the photocatalytic mechanism.

Overall, the results underscore the promise of Sr- and Cr-modified PEO coatings on Mg alloys as viable materials for photocatalytic wastewater treatment applications.

References

1. I.K. Konstantinou, T.A. Albanis, TiO2-assisted photocatalytic degradation of azo dyes in aqueous solution: kinetic and mechanistic investigations, Appl. Catal. B Environ. 49 (2004) 1–14.
2. D. Mouloua, M. Lejeune, N.S. Rajput, K. Kaja, M. El Marssi, M.A. El Khakani, M. Jouiad, One-step chemically vapor deposited hybrid 1T-MoS2/2H-MoS2 heterostructures towards methylene blue photodegradation, Ultrason. Sonochem. 95 (2023) 106381.
3. H. Widiyandari, O. Prilita, M.S. Al Ja'farawy, F. Nurosyid, O. Arutanti, Y. Astuti, N. Mufti, Nitrogen-doped carbon quantum dots supported zinc oxide (ZnO/N-CQD) nanoflower photocatalyst for methylene blue photodegradation, Results Eng. 17 (2023) 100814.
4. P.O. Oladoye, T.O. Ajiboye, E.O. Omotola, O.J. Oyewola, Methylene blue dye: Toxicity and potential elimination technology from wastewater, Results Eng. 16 (2022) 100678.
5. A. Norouzi, A. Nezamzadeh-Ejhieh, Investigation of the simultaneous interactions of experimental variables and mechanism pathway in the photodegradation of methylene blue by binary ZnO/Cu2O photocatalyst, Mater. Res. Bull. 164 (2023) 112237.
6. W. Liu, Y. Lu, Y. Dong, Q. Jin, H. Lin, A critical review on reliability of quenching experiment in advanced oxidation processes, Chem. Eng. J. 466 (2023) 143161.
7. S.-W. Lv, Y. Cong, X. Chen, W. Wang, L. Che, Developing fine-

tuned metal–organic frameworks for photocatalytic treatment of wastewater: A review, Chem. Eng. J. 433 (2022) 133605.
8. M. Coto, S.C. Troughton, P. Knight, R. Joshi, R. Francis, R.V. Kumar, T.W. Clyne, Optimization of the microstructure of TiO2 photocatalytic surfaces created by Plasma Electrolytic Oxidation of titanium substrates, Surf. Coatings Technol. 411 (2021) 127000.
9. P. Properties, MgAl Oxide Coatings Modified with CeO 2 Particles Formed by Plasma Electrolytic Oxidation of AZ31 Magnesium Alloy :, (2024).
10. W. Li, M. Tang, L. Zhu, H. Liu, Formation of microarc oxidation coatings on magnesium alloy with photocatalytic performance, Appl. Surf. Sci. 258 (2012) 10017–10021.
11. Y. Jiang, K. Huang, W. Ling, X. Wei, Y. Wang, J. Wang, Investigation of the Kinetics and Reaction Mechanism for Photodegradation Tetracycline Antibiotics over Sulfur-Doped Bi 2 WO 6-x / ZnIn 2 S 4 Direct Z-Scheme Heterojunction, (2021).
12. S. Zhong, C. Li, M. Shen, C. Lv, S. Zhang, Synthesis of modified bismuth tungstate and the photocatalytic properties on tetracycline, Integr. Med. Res. 8 (2019) 1849–1858.
13. A. El Aouni, M. El Ouardi, M. Arab, M. Saadi, Z. Kónya, A. Ben Ali, A. Jada, A. Baqais, A. El Aouni, M. El Ouardi, M. Arab, M. Saadi, H. Haspel, Design of Bismuth Tungstate Bi2WO6 Photocatalyst for Pollutant Degradation To cite this version : HAL Id : hal-04482548, (2024).
14. H.F. Guo, M.Z. An, Growth of ceramic coatings on AZ91D magnesium alloys by micro-arc oxidation in aluminate–fluoride solutions and evaluation of corrosion resistance, Appl. Surf. Sci. 246 (2005) 229–238.
15. P. Su, X. Wu, Y. Guo, Z. Jiang, Effects of cathode current density on structure and corrosion resistance of plasma electrolytic oxidation coatings formed on ZK60 Mg alloy, J. Alloys Compd. 475 (2009) 773–777.
16. A. Fardosi, A. Fattah-alhosseini, M. Karbasi, R. Chaharmahali, B. Dikici, Improved electrochemical stability of AZ31B magnesium alloy via PEO surface films with strontium and chromium additives at different current densities, Surf. Coat. Technol. 515 (2025) 132681.
17. R.D. Shannon, C.T. Prewitt, Revised values of effective ionic radii, Acta Crystallogr. Sect. B Struct. Crystallogr. Cryst. Chem. 26 (1970) 1046–1048.
18. C.G. Pope, X-Ray Diffraction and the Bragg Equation, J. Chem. Educ. 74 (1997) 129.
19. H. Mozafarnia, A. Fattah-Alhosseini, R. Chaharmahali, M. Nouri, M.K. Keshavarz, M. Kaseem, Corrosion, Wear, and Antibacterial Behaviors of Hydroxyapatite/MgO Composite PEO Coatings on AZ31 Mg Alloy by Incorporation of TiO2 Nanoparticles, Coatings 12 (2022) 1967.
20. E. Vazirinasab, R. Jafari, G. Momen, Application of superhydrophobic coatings as a corrosion barrier: A review, Surf. Coatings Technol. 341 (2018) 40–56.
21. S. Arun, P.N. Sooraj, S. Hariprasad, T. Arunnellaiappan, N. Rameshbabu, Fabrication of superhydrophobic coating on PEO treated zirconium samples and its corrosion resistance, Mater. Today Proc. 27 (2019) 2056–2060.
22. R. Luo, Y. Jiao, S. Zhang, J. Wu, X. Wu, K. Lu, P. Zhang, Y. Li, X. Ni, Q. Zhao, Fabrication, properties and biological activity of a titanium surface modified with zinc via plasma electrolytic oxidation, Front. Mater. 10 (2023).
23. Y. Qiao, D. Zhang, Z. Yang, Z. Zhu, X. Lu, B. Ou, J. Zhang, S. Jin, Q. Wang, K. Yu, Structural characterization and biological compatibilities of PEO coated Ti–Mg metal matrix composites, J. Mater. Res. Technol. 30 (2024) 2911–2921.
24. H.Y. Erbil, C.E. Cansoy, Range of Applicability of the Wenzel and Cassie - Baxter Equations for Superhydrophobic Surfaces †, 25 (2009) 14135–14145.
25. G. Mchale, N.J. Shirtcliffe, M.I. Newton, Contact-Angle Hysteresis on Super-Hydrophobic Surfaces, (2004) 10146–10149.